JOURNAL OF SOLID STATE CHEMISTRY 37, 49–57 (1981)

An Electron Microscope Study on Substitutional Order and Disorder in the System MnS–Ln_2S_3 (Ln = Yb or Y)

M. BAKKER AND C. M. PLUG

Gorlaeus Laboratories, State University, P.O. Box 9502, 2300 RA Leiden, The Netherlands

Received March 10, 1980; in revised form May 29, 1980

The substitution of 2 Ln^{3+} (Ln is Yb or Y) for $3Mn^{2+}$ at about 1873 K in the α-MnS structure (cubic close packing) was investigated by means of electron diffraction (at room temperature). Diffuse intensity contours suggest that clusters of Mn^{2+} and Ln^{3+} around a vacancy are formed. In the close-packed plane, the cluster is a hexagon of $4Mn^{2+}$ and $2Ln^{3+}$ around a vacancy, a seven-point cluster. Clusters remain independent up to composition $4MnS \cdot Ln_2S_3$. With higher Yb_2S_3 content spinel domains in the short-range-order matrix are formed. Samples of MnS–Y_2S_3 heated at 1873 K showed formation of extended defects (in this case twin planes) when they contained more than 20 mole% Y_2S_3 (14% vacancies).

Introduction

For many years it has been known that nonmolecular crystalline solids can accommodate disorder and changes of composition by forming so-called "extended defects" (*1*). These defects may be formed by, for example, crystallographic shear or mimetic twinning, but also by other operations (*2*). The effect of mimetic twinning is apparent in the system MnS–Y_2S_3 (*3*). In this system, where $3Mn^{2+}$ are substituted by $2Y^{3+}$ in the fcc structure of α-MnS, the occurrence of extended defects, in this case twin planes, eliminated the need for a random vacancy model proposed by earlier investigators (*4*). The formation of extended defects appears to occur only below 1673 K. For a description of the system at higher temperatures (about 1873 K), a point–defect model still may be considered.

For the system MnS–Yb_2S_3 an extended MnS-type solid solution has also been reported (*4*). $MnYb_2S_4$, however, crystallizes in the spinel structure, which cannot be derived from the rock salt structure by shear or twinning. Therefore, it is not likely that the structure of this solid solution is also based on extended defects. A point–defect model has to be considered. As almost 15% vacancies would occur in these compounds, it seems unlikely that these, together with Mn^{2+} and Ln^{3+}, would be randomly distributed over the cation lattice. In the last 7 years, electron and X-ray diffraction studies on a number of binary alloys (*5, 6*), on some transition metal carbides (*7–9*) and some ionic compounds as $LiFeO_2$ (*10*) or $LiTbS_2$ (*11*), all having a rock salt-type structure, revealed diffuse intensity contours in the diffraction patterns due to short-range ordering.

It is this kind of ordering that is expected in the structure of MnS, when Y_2S_3 or

0022-4596/81/040049-09$02.00/0

Yb_2S_3 is substituted. Therefore, a number of samples, varying in composition and preparation temperature, were investigated by electron microscopy diffraction.

Diffuse Scattering

In general, in a real crystal, clustering, local order, short-range order, and mean-square and thermal displacements cause X-ray, electron, or neutron scattering, in addition to the Bragg reflections of the average lattice. Recorded intensity provides information on parameters describing these phenomena, e.g., the order parameter α for short-range order (SRO) defined by Warren and Cowley (*12*). General equations for diffuse scattering (*13*) indicate that the diffuse scattering arising from SRO is always located between Bragg peaks. Intensity due to displacements is of the same order of magnitude and can be located near the SRO contours, near Bragg reflections, or even under the Bragg peaks. This makes the interpretation of diffuse intensity contours very complicated.

The state between SRO and LRO (long-range order), when the diffuse intensity distribution changes from three dimensional to zero dimensional (concentrating into superlattice reflections of the LRO structure) is called the "transition state" (*14*). In the transition state, which is a prefiguration of the LRO structure, the diffuse intensity is mostly restricted to a line or a surface in reciprocal space. For electron diffraction, the kinematical theory, which gives good results for X-ray diffuse scattering, applies only in first approximation. Furthermore, it is difficult to record the exact diffuse scattering intensity with the electron microscope. It is, however, fairly easy to obtain its geometrical distribution.

The use of only the geometry of the diffuse scattering distribution, together with the idea that the geometry is not affected by dynamical scattering, is a basis for the "cluster theory," The expression

$$A_d(\bar{g}) \cdot f(\bar{g}) = 0 \qquad (1)$$

states that the diffuse scattering amplitude $A_d(\bar{g})$ can only be different from zero on a surface $f(\bar{g}) = 0$ ($\bar{g}$ is a vector in reciprocal space). The scattering amplitude can be written as

$$A_d(\bar{g}) = \sum_j \sigma_j \cdot \exp 2\pi i(\bar{g} \cdot \bar{r}_j). \qquad (2)$$

In Eq. (2), σ_j are the occupation operators for the positions $\bar{r}_j$. The locus $f(\bar{g})$ can be written by the Fourier representation

$$f(\bar{g}) = \sum_k \omega_k \cdot \exp\left(-2\pi i(\bar{g} \cdot \bar{r})\right). \qquad (3)$$

In Eq. (3), ω_k are the Fourier components for the positions $\bar{r}_k$. Substitution of Eqs. (2) and (1) leads to the so-called "cluster" relation

$$\sum_k \omega_k \cdot \sigma_{j+k} = 0. \qquad (4)$$

It shows that there are polyhedra (octahedra or tetrahedra, for example) in the structure for which the occupation vectors (σ_j) are correlated (*15, 16*). If all Fourier coefficients in Eq. (4) are equal to 1 ($\Sigma_k \sigma_{j+k} = 0$) it indicates that the polyhedra have macroscopic composition.

From an analytical expression, describing the geometry of the experimental scattering distribution, it is thus possible to determine the polyhedral building blocks, which are characteristic for the transition state. Many structures are based on building blocks other than the unit cell; for example, ccp structures can be thought to be built by a regular arrangement of tetrahedra (Cu_2Au_2, Cu_3Au) or centered octahedra (VC, $LiFeO_2$, $LiTbS_2$) (*8, 9,17*). The variables for a structure in the transition state are the composition[1] and the

[1] Mostly in the transition state, a majority of clusters will have the macroscopic composition.

configuration[2] of the polyhedral building blocks. A polyhedron with a specific configuration and composition is called a "cluster." In high-symmetry structures another variable is the mutual arrangement of the clusters. In the transition state this amount of freedom gradually decreases, which means that one or two types of cluster will become predominant and that the cluster arrangement will become locally ordered. In fact, microdomains with two or three times the unit-cell dimension, having the LRO structure, are formed. Growth of these domains will gradually decrease the concentrations of other (different) clusters in the domain boundaries.

When displacive diffuse scattering is located between Bragg reflections, a similar approach is possible (*18*). The diffuse intensity contours are then correlated to a weighted sum of vector displacements of atoms within the cluster that is defined by the geometrical surface of diffuse intensity. The cluster model will be used to describe the diffuse intensity contours observed by electron diffraction in MnS doped with Y_2S_3 or Yb_2S_3 and to discuss the ordering state in these systems.

Experimental

α-MnS, the rare-earth sulfide Yb_2S_3, and Y_2S_3 were prepared by heating the oxides, contained in graphite crucibles, using a rf induction furnace, in a stream of H_2S gas. The diffraction patterns of the sulfides were recorded on a Philips powder diffractometer (Cu$K\alpha$, λ = 1.5418 Å). Various mixtures of MnS with the sesquisulfides of Y and Yb (5/1–1/1) were similarly heated for about 20 min at the melting point (dependent on composition between 1773 and 1873 K) and air-cooled. After examination by X-ray diffraction the samples were crushed in liquid nitrogen, dispersed in alcohol, and mounted on a 400-mesh copper grid, coated with Formvar/carbon Holey film. These were examined in a Siemens Elmiskop 102, fitted with a double tilt and lift cartridge, and operating at 100 and 125 kV. To be able to determine lattice constants from electron micrographs, the camera constant λL was calibrated versus the objective current using an Al-film. Images were recorded on Kodak Electron Image plates and developed for 7 min in D19.

Results

(*a*) *X-Ray Diffraction*

The powder diffraction results for mixtures of MnS with Ln_2S_3 (*Ln* is Y or Yb) were in accordance with those previously reported (*4*). At 1873 K the 1/1 mixtures formed compounds $MnLn_2S_4$, while the 2/1 and 3/1 gave the stoichiometric 1/1 compounds plus nonstoichiometric rock salt-type phases. The cubic axes of these phases are consistent with values for the maximum solubility of Ln_2S_3 in MnS at this temperature. Mixtures with lower Ln_2S_3 concentration formed only nonstoichiometric NaCl-type phases. For example, the composition $4MnS \cdot Y_2S_3$ forms a phase with a = 5.375(3) Å. The broad peaks in the powder diffraction pattern indicate, however, that this value is actually an average.

$MnYb_2S_4$ crystallizes with a normal spinel structure (x = 0.375(4),[3] a = 10.949(6) Å) (*19*). The structure of MnY_2S_4 is orthorhombic and can be described as mimetic twinned ccp (*3*). The c axis is thus approximately $8 \times d_{113}$. The reported unit-cell axes are a = 3.78(1), b = 12.62(1), and c = 12.75(1) Å (*20*).

[2] There are, for example, *two* A_3B_3 octahedral configurations and *five* A_4B_4 cube cluster configurations (*8*, *9*).

[3] x is the parameter for the anion positions in spinel. $x = 3/8 + \mu$, in which μ is a rate for the deviation from cubic close packing.

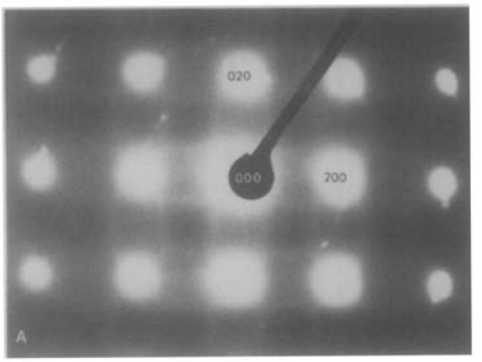

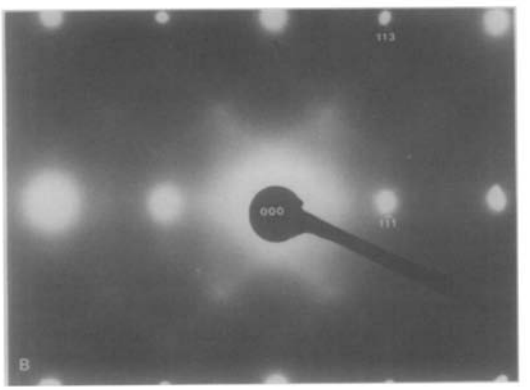

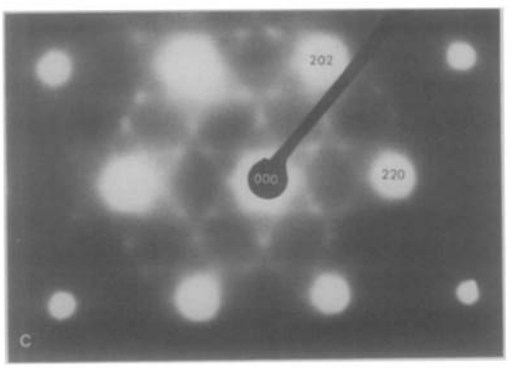

FIGS. 1A, B, C. The ⟨100⟩, ⟨112⟩, ⟨111⟩ reciprocal lattice sections from crystals with average composition $4MnS \cdot Ln_2S_3$. Indices refer to a rock salt-type unit cell. Diffuse scattering due to a transition state is visible.

(*b*) *Electron Microscopy/Diffraction*

1. $MnS-Yb_2S_3/Y_2S_3$. Composition 5/1–4/1. In this composition range the results for Yb^{3+} and Y^{3+} are similar. Several reciprocal lattice sections from single crystals

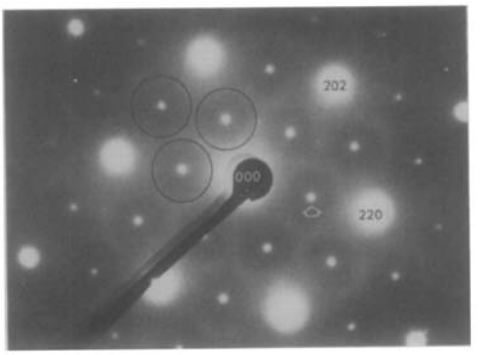

FIG. 2. The ⟨111⟩ reciprocal lattice section from a crystal with average composition $3MnS \cdot Yb_2S_3$. Besides diffuse scattering, which for clarity has been indicated by circles superreflections due to spinel domains are visible. The indices also refer to a rock salt-type unit cell ($a = \frac{1}{2}a$ (spinel)).

were obtained using a double tilt and lift device in the electron miscroscope. Three typical sections, for crystals with average composition 4/1, the ⟨100⟩, ⟨112⟩, and the ⟨111⟩ (fcc) are shown in Figs. 1a, b, and c. Between the Bragg reflections of the average MnS-type structure there are distinct diffuse intensity contours. In the ⟨100⟩ and ⟨112⟩ sections there is also strong diffuse scattering near the Bragg peaks. The unit-cell axes, calculated from the Bragg reflections, of the average structure was used as a standard for determining the composition of the different samples. The intensity of the diffuse scattering appears to vary with the composition, whereas the geometry of the intensity distribution also changes slightly with increasing Ln^{3+} concentration.

2. $MnS-Yb_2S_3$. Composition 3/1. Figure 2 is the ⟨111⟩ reciprocal lattice section. For this composition both diffuse scattering and superreflections are observed between the main reflections. A dark field image, using the superreflection, indicated by the arrow, in Fig. 2, reveals a domain texture of 40–60 Å (Fig. 3). Another feature is the geometry of the diffuse intensity distribution in Fig. 2, which is clearly different from

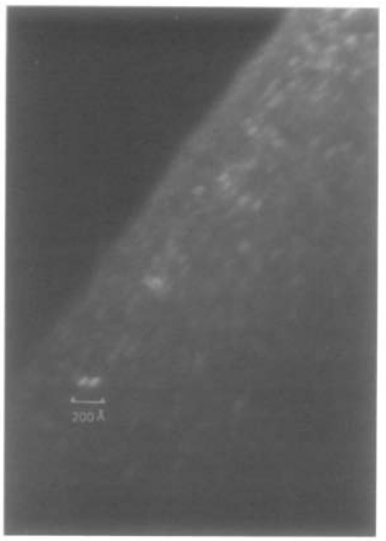

FIG. 3. A dark-field image using the reflection indicated by the arrow in Fig. 2. The domains extend over 40–60 Å.

but still comparable with the one in Fig. 1c.

3. $MnS–Y_2S_3$. Composition 3/1. In the selected area diffraction patterns from crystals having this average composition again diffuse intensity contours occur. In addition, in some diffraction patterns extra spots (Fig. 4, ⟨111⟩), in other diffuse lines (streaking) along $\bar{g}(113)$ (Fig. 5, ⟨013⟩), are observed. In the corresponding micrograph of the ⟨013⟩ section (Fig. 6) groups of planar defects are visible, which intersect slabs of nonstoichiometric "MnS." The one-dimensional diffuse scattering (a line) and the two-dimensional contours are clearly different in nature.

4. $MnS–Yb_2S_3/Y_2S_3$. Composition 2/1–1/1. In this composition range mostly $MnYb_2S_4$- or MnY_2S_4-type diffraction patterns were found. In the case of Yb^{3+} there is an increase in the intensity of the superreflection from 2/1 toward 1/1. For Y^{3+} in some diffraction patterns of the MnY_2S_4-type one-dimensional diffuse scattering is observed. The two-dimensional contours can no longer be detected, the contributing regions being too small.

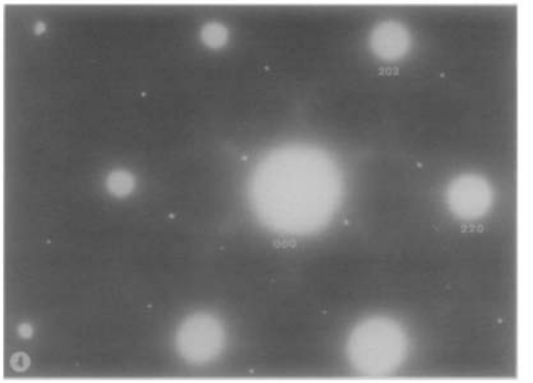

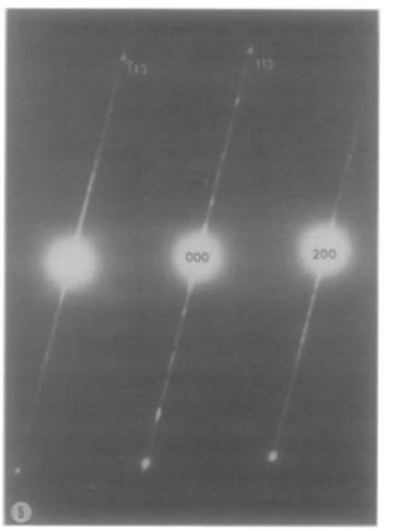

FIGS. 4, 5. The ⟨111⟩ and ⟨013⟩ selected area diffraction patterns from single crystals with average composition $3MnS \cdot Y_2S_3$. Streaking along $\bar{g}(113)$ is seen in both images. Indexing of the reflections is based on a NaCl-type unit cell.

Discussion

Substitution of Yb_2S_3 or Y_2S_3 into α-MnS will result in a distribution of Mn^{2+} ions, Yb^{3+} (Y^{3+}) ions, and cation vacancies (due to charge compensation: $3Mn^{2+} \leftarrow 2Yb^{3+} + 1\square$) over the available cations sites formed by close-packed sulfur atoms. The observed diffuse intensity contours indicate this distribution to be nonrandom. Information concerning the nature of the cation distribution can be extracted from the geometry of the diffuse intensity contours,

FIG. 6. Micrograph corresponding to Fig. 5. Groups of planar defects (twin planes) are more or less randomly distributed over the "MnS" matrix.

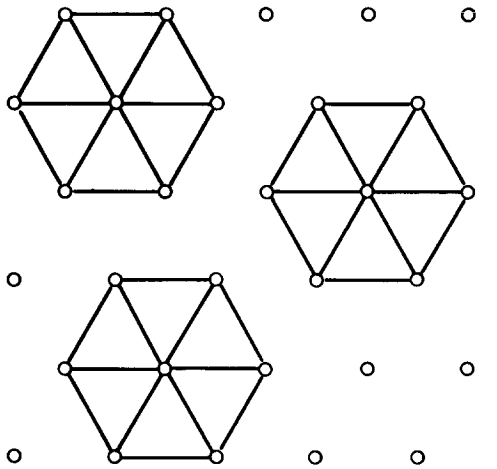

FIG. 7. Cation sites in a close-packed layer. Three isolated seven-point clusters are drawn.

without detailed knowledge of the intensities. In this case it is convenient to consider, for composition 4/1, the two-dimensional distribution in the ⟨111⟩ reciprocal lattice section (Fig. 1c), which provides information on the occupation of the cations in close-packed layers. The structure of the nonstoichiometric MnS phase can be built by stacking these layers in sequence A, B, C.

The locus of diffuse intensity in the ⟨111⟩ section is represented by

$$f(\bar{g}) = 1 + 2\{\cos 2\pi k + \cos 2\pi h + \cos 2\pi(h + k)\} + \alpha, \quad (5)$$

in which $\alpha = 0.8$. The parameter α will be discussed later. From Eq. (5) using the Eqs. (1)–(4) above, the following seven vectors may be derived: (0,0), (0,1), (1,0), (1,1), (0,$\bar{1}$), ($\bar{1}$,0), and ($\bar{1}$,$\bar{1}$). Together they define isolated centered hexagons in the {111} fcc plane (Fig. 7). In the cluster relation, Eq. (4), all the ω_k equal 1, which states that the seven-point clusters all have macroscopic composition ($4Mn^{2+}$, $2Ln^{3+}$, 1□) (*15, 16*). This satisfies the condition for charge compensation and agrees with the bulk composition of the samples.

If a vacancy is located in the center, then there are 15 possibilities of placing $4Mn^{2+}$, $2Ln^{3+}$ on the corners of the hexagon. Thus 15 configurations or clusters are possible. With respect to the mutual positions of the trivalent cations, three configurations can be denoted by *para*, six by *meta*, and six by *ortho*. The charge distribution will undoubtedly favor the *para* configurations (clusters), and in the structure these will be predominant. This feature is manifested in the nonhomogeneous distribution of diffuse intensity. To determine the precise fraction of each cluster occurring, one should know the exact intensity.

The experiments showed that decreasing the Yb^{3+} or Y^{3+} concentration did not alter the geometry of the diffuse scattering distribution, except for some minor changes, due to displacements, which will be discussed hereafter. This implies that even at the lowest Ln^{3+} concentration the same clusters will still be formed in the nonstoichiometric "MnS" structure, i.e., that there are two trivalent cations surrounding a vacancy.

The parameter α is correlated to a deformation of the locus observed in Fig. 1c. When $\alpha = 0.0$ the corresponding cluster would be a perfect centered hexagon. Comparison of several calculated loci with the one observed indicates α to be approximately 0.8 (see Figs. 8a and b). The deformation of the locus is related to displacements in the cation lattice. These displacements are, however, correlated within groups of seven atoms (the cluster) (*18*). Observations suggest that the magnitude of the displacements depends on the Ln^{3+} concentration (the lower the concentration the smaller the deformations). Of course, the anion lattice will suffer under these movements. The anions, especially those near a vacancy, will also move, first in order to accommodate the larger Ln^{3+} cations, and second because of interanionic repulsions around a vacancy. This displacement field is thought to be responsible for observed diffuse scattering near the Bragg peaks (Figs. 1a and b). So far, it has not been possible to find a more quantative description.

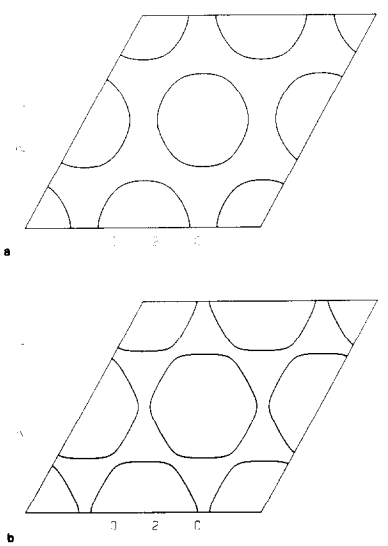

FIGS. 8A, B. Calculated loci for $\alpha = 0.0$ and 0.8, respectively, using Eq. (3).

The planar seven-point clusters can no longer stay isolated when the Ln^{3+} concentration increases beyond 28 mole% (composition 4/1). Indeed, in the case of MnS and Yb_2S_3 small regions of spinel-type structure[4] in the "MnS" matrix are formed (composition 3/1, 2/1), which give rise to superreflections as in Fig. 2. These domains extend over about 40–60 Å. The diffuse intensity distribution is now described well with $\alpha = 0.0$. Clearly, in the "transition state MnS" there are no longer displacements, with respect to the original cation lattice. At higher Yb^{3+} concentrations the spinel structure will start to dominate over the "MnS" structure.

$MnS \cdot Y_2S_3$ samples with the Y^{3+} concentration above the critical 28% show formation of extended defects. In the diffraction pattern the more or less randomly distributed defects produce streaking along $\bar{g}(113)$ (Fig. 5). In the $\langle 111 \rangle$ zone (Fig. 4) the streaks intersect with the Ewald sphere forming a misleading regular spot pattern (no superreflections). Recent investigations (*3*) showed that these planar defects are twin planes. In Fig. 6 they intersect slabs of the "MnS"-type structure. These exsolution twin planes are always formed in pairs.[5] The two-dimensional intensity distribution has not changed in this case; α is still 0.8. The deformation is apparently the same as that in the original "MnS"-type structure.

Applying the cluster theory to the observed diffuse intensity contours in the $\langle 111 \rangle$ reciprocal lattice section, a description of the ordering state in the $\{111\}$ fcc planes is derived. It is possible to extend the description of the ordering state to the whole three-dimensional structure, still with the vacancy-centered hexagon as the

[4] In the spinel structure Yb^{3+} occupies an octahedron and Mn^{2+} a tetrahedron, according to Paulings rule (*21*), in a ccp sulfur matrix.

[5] Only a growth twin can occur singly.

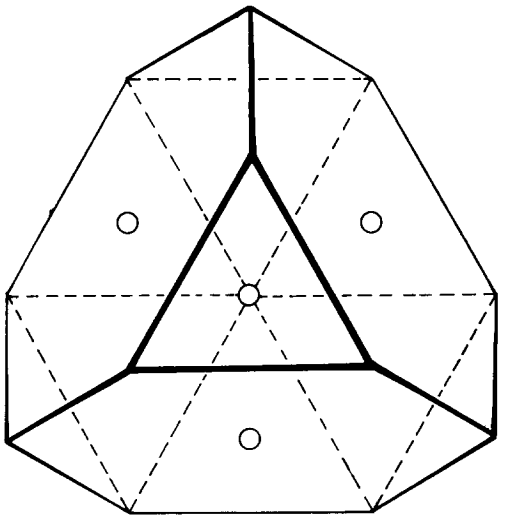

FIG. 9. Truncated tetrahedron formed by four intersecting hexagons.

basic cluster, using the truncated tetrahedron. One can think of the truncated tetrahedron as formed by intersecting hexagons (Fig. 9) which are oriented along the equivalent {111} planes of the ccp structure. Using the polyhedron it is easy to see how spinel domains (in the case of Yb^{3+} substitution) can eventually precipitate within the MnS matrix, when the Yb/Mn ratio increases. Eliminating $3Mn^{2+}$ from a seven-point cluster step by step and replacing them by $2Y^{3+}$ and a vacancy in each of the {111} planes, a situation will finally arise in which four vacancy-centered hexagons intersect, forming a truncated tetrahedron with four vacant sites. When a Mn^{2+} is placed in the center of this polyhedron a cation distribution evolves, which is also found in the structure of Cu_2Mg, being the cation lattice in the spinel structure. This process can obviously not account for the formation of twin planes in the case of Y^{3+} substitution. The formation of twin planes is governed by changes in the anion lattice rather than by a rearrangement of the cation distribution.

Conclusion

The cluster theory is able to explain most of the diffuse scattering phenomena observed due to the substitution of Ln_2S_3 (*Ln* is Yb or Y) in MnS. From the scattering distribution it can be derived that vacancies are formed, which are surrounded by a hexagonal cluster of Mn^{2+} and Ln^{3+} cations. The degrees of freedom for a cluster, like those of composition and configuration, are characterisic for the transition state. As the intensity has not been recorded, no complete description can be given, i.e., the concentration of different clusters occurring in the structure. Yet the inhomogeneous distribution of the intensity on the locus indicated a preference for one type of cluster. Despite this preference no superstructures based on the seven-point cluster[6] have been found in this system. Superstructures based on a seven-point cluster do occur in some intercalate systems. For example, the systems Cu_xNbS_2 (*23*) and Na_xVSe_2 (*24, 25*) give diffraction results which are similar to those of the ⟨111⟩ section in the $MnS \cdot Ln_2S_3$ system. The results also indicate that the description of solid solutions, in terms of random distribution, is not always adequate. Even when heated to very high temperatures and when rapidly cooled, no absolute disorder exists in the $MnS \cdot Ln_2S_3$. It is likely that similar phenomena in other substitutional systems, ternary oxides, and sulfides will be revealed.

[6] The observed spinel structure is in terms of the theory described under Diffuse Scattering, not a superstructure based on the seven-point cluster, because a second (tetrahedral) lattice becomes involved. Consequently, the spinel reflection is not located on the locus describing the diffuse intensity distribution.

References

1. A. D. WADSLEY, *in* "Non-Stoichiometric Com-

pounds" (L. Mandelcorn, Ed.), p. 98, Academic Press, New York (1964).
2. B. G. HYDE, A. N. BAGSHAW, S. ANDERSON, AND M. O'KEEFFE, *Ann. Rev. Mater. Sci.* **4**, 43 (1974).
3. M. BAKKER AND B. G. HYDE, *Phil. Mag. A* **38**, 615 (1978).
4. J. FLAHAUT, *in* "Progress in the Science and Technology of the Rare Earths" (L. Eyring, Ed.), Vol. 3, p. 236, Pergamon, New York (1968).
5. K. I. OSHIMA AND D. WATANABE, *Acta Crystallogr. Sect. A* **29**, 520 (1973).
6. K. I. OSHIMA AND D. WATANABE, *Acta Crystallogr. Sect. A* **33**, 784 (1977).
7. J. BILLINGHAM, P. S. BELL, AND M. H. LEWIS, *Acta Crystallogr. Sect. A* **28**, 602 (1972).
8. M. SAUVAGE AND E. PARTHÉ, *Acta Crystallogr. Sect. A* **28**, 607 (1972).
9. M. SAUVAGE AND E. PARTHÉ, *Acta Crystallogr. Sect. A* **30**, 239 (1974).
10. M. BRUNEL, F. DE BERGEVIN, AND M. GONDRAND, *J. Phys. Chem. Solids.* **33**, 1927 (1972).
11. C. M. PLUG AND A. PRODAN, *Acta Crystallogr. Sect. A* **34**, 250 (1978).
12. J. M. COWLEY, *J. Appl. Phys.* **21**, 24 (1950).
13. M. HAYAKAWA AND J. B. COHEN, *Acta Crystallogr. Sect. A* **31**, 635 (1975).
14. R. DE RIDDER, G. VAN TENDELOO, AND S. AMELINCKX, *Acta Crystallogr. Sect. A* **32**, 216 (1976).
15. R. DE RIDDER, G. VAN TENDELOO, D. VAN DYCK, AND S. AMELINCKX, *Phys. Status Solidi A* **43**, 541 (1977).
17. E. W. GORTER, *J. Solid State Chem.* **1**, 279 (1970).
18. R. DE RIDDER, D. VAN DYCK, AND S. AMELINCKX, *Phys. Status Solidi A* **50**, 349 (1978).
19. M. PATRIE, J. FLAHAUT, AND L. DOMANGE, *C.R. Acad. Sci. Paris Ser. C* **258**, 2585 (1964).
20. M. PATRIE AND R. CHEVALIER, *C.R. Acad. Sci. Paris Ser. C* **263**, 1061 (1966).
21. L. PAULING, "The Nature of the Chemical Bond," 3rd ed., p. 547, Cornel Univ. Press, Ithaca, N.Y. (1971).
22. M. J. WENNINGER, "Polyhedron Models," Univ. Press, Cambridge, 1971.
23. R. DE RIDDER, G. VAN TENDELOO, J VAN LANDUYT, D. VAN DYCK, AND S. AMELINCKX, *Phys. Status Solidi A* **37**, 591 (1976).
24. C. F. VAN BRUGGEN, C. HAAS AND G. A. WIEGERS, *J. Solid State Chem.* **27**, 9 (1979).
25. J. VAN LANDUYT, G. A. WIEGERS, AND S. AMELINCKX, *Phys. Status Solidi A* **46**, 479 (1978).